Iris Recognition

by

Frankin Cheung

Department of Computer Science and Electrical Engineering

The University of Queensland

Submitted for the degree of

Bachelor of Engineering (PASS)

In the division of Computer Systems Engineering

October 1999

6 Kolan Street

Runcorn 4113

Tel.(07) 3273 5170

October 13,1999

The Dean

School of Engineering

University of Queensland

St Lucia, Qld 4072

Dear Professor Simmons,

In accordance with the requirements of the degree of Bachelor of Engineering (PASS) in the division of Computer Systems Engineering, I present the following thesis entitled "Iris Recognition". This work was performed by myself under the supervision of Dr. Brian Lovell.

I declare that the work submitted in this thesis is my own, except as acknowledged in the text and footnotes, and has not been previously submitted for a degree at the University of Queensland or any other institution.

Yours sincerely,

Frankin Cheung

To…

Acknowledgements

Many thanks go to those who made this thesis possible, including:

Dr Brian Lovell for providing such a great facility like Signal Processing Lab, which made a lot of other student who don't have it very jealous. His guidance was always well received, as was his tolerance regarding persistent interruptions and demand for help.

Andrew Over for all his encouragement at any given time, and in any form. Without his encouragement, I would have suffered from too much stress, and would have given up in a lot of the times.

Graeme Saunders for his effort of making the 24 hours weekday access possible and his occasional free humorous chats.

Juergen Marchard for everything from maintaining my computer network functionality to making coffee.

Contents

Abstract

A study of a human recognition by use of biometrics known as Iris Recognition is provided. Based on the technology invented by Dr. John G. Daugman, an attempt of implementing a workable system was made. Although the attempt did not succeed in every aspect, "Iris Recognition" is forecast to play a role in a wide range of other applications in which a person's identity must be established or confirmed. These include passport control, electronic commerce, entitlements payments, premises entry, access to privileged information, authorizations, forensic and police applications, computer login, or any other transaction in which personal identification currently relies just on special possessions or secrets (keys, cards, documents, passwords, PINs).

Chapter 1

1 Introduction

Identification of humans is a goal as ancient as humanity itself. As technology and services have developed in the modern world, human activities and transactions have proliferated in which rapid and reliable personal identification is required. Examples include passport control, computer login control, bank automatic teller machines and other transactions authorization, premises access control, and security systems generally. All such identification efforts share the common goals of speed, reliability and automation.

The use of biometric indicia for identification purposes requires that a particular biometric factor be unique for each individual that it can be readily measured, and that it is invariant over time. Biometrics such as signatures, photographs, fingerprints, voiceprints and retinal blood vessel patterns all have significant drawbacks. Although signatures and photographs are cheap and easy to obtain and store, they are impossible to identify automatically with assurance, and are easily forged. Electronically recorded voiceprints are susceptible to changes in a person's voice, and they can be counterfeited. Fingerprints or handprints require physical contact, and they also can be counterfeited and marred by artifacts.

Human iris on the other hand as an internal organ of the eye and as well protected from the external environment, yet it is easily visible from within one meter of

distance makes it a perfect biometric for an identification system with the ease of speed, reliability and automation.

In this thesis, we are going to experiment, implement, and most importantly, look into the theory behind an Iris Recognition System, which is not only related to the filed of personal identification, and more specifically to the field of automated identification of humans by biometric indicia

Chapter 2

2 Why is Iris Recognition possible?

2.1 History

Efforts to devise reliable mechanical means for biometric personal identification have a long and colorful history. However, the idea of using iris patterns for personal identification was originally proposed in 1936 by ophthalmologist Frank Burch, MD. In the 1980's the idea appeared in James Bond movies, but it remained science fiction. It was not until 1987, two American ophthalmologists, Leonard Flom and Aran Safir patented Burch's concept but they were unable to develop such a process. So Instead they turned to John Daugman, who was teaching at Harvard University and now at Cambridge University, to develop actual algorithms for iris recognition. These algorithms, which Daugman developed in 1994, are the basis for all current iris recognition systems.

2.2 Properties of an Iris

The critical attributes for any biometrics are: the number of degree-of-freedom of variation in the chosen index across the human population, since this determines uniqueness; its immutability over time and its immunity to intervention; and the computational prospects for efficiently encoding and reliably recognizing the

identifying pattern. In the entire human population, no two irises are alike in their mathematical detail, even among identical (monozygotic) twins. The probability that two irises could produce exactly the same Iris Code is approximately 1 in 10^{78}. (The population of the earth is around 10^{10} .)

The possibility that the iris of the eye might be used as a kind of optical fingerprint for personal identification was suggested originally by ophthalmologists [1], [12], [24], who noted from clinical experience that every iris had a highly detailed and unique texture, which remained unchanged in clinical photographs spanning decades. The iris is composed of elastic connective tissue, the trabecular meshwork, whose prenatal morphogenesis[1] is completed during the 8th month of gestation. It consists of pectinate ligaments adhering into a tangled mesh revealing striations, ciliary processes, crypts, rings, furrows, a corona, sometimes freckles, vasculature, and other features. During the first year of life a blanket of chromatophore cells usually changes the color of the iris, but the available clinical evidence indicates that the trabecular pattern itself is stable throughout the lifespan.

Properties that enhance its suitability for use in automatic identification include: its inherent isolation and protection from the external environment, being an internal organ of the eye, behind he cornea and the aqueous humor; the impossibility of surgically modifying it without unacceptable risk to vision and its physiological response to light, which provides a natural test against artifice.

A Property the iris shares with fingerprints is the random morphogenesis of its minutiae. Because there is no genetic penetrance in the expression of this organ beyond its anatomical form, physiology, color and general appearance, the iris texture itself is stochastic or possibly chaotic. Since its detailed morphogenesis depends on initial conditions in the embryonic mesoderm from which it develops [11], the phenotypic expression even of two irises with the same genetic genotype (as in identical twins, or the pair possessed by one individual) have uncorrelated minutiae. In these respects the uniqueness of every iris parallels the uniqueness of every fingerprints, common genotype or not. But the iris enjoys further practical advantages

---

[1] the processes that are responsible for producing the complex shapes of adults from the simple ball of cells that derives from division of the fertilized egg

over fingerprints and other biometrics for purposes of automatic recognition, including the ease of registering its image at some distance from the Subject without physical contact unintrusively and perhaps inconspicuously and its intrinsic polar geometry, which imparts a natural coordinate system and an origin of coordinates.

The following chapter will present the theory behind a working model of iris recognition system invented by Dr John G Daugman.

Chapter 3

3   Theory

In Dr John G. Daugman's paper, patent number: 5,291,560 released on Mar. 1, 1994, the procedures of an iris recognition system is described in Figure 1.
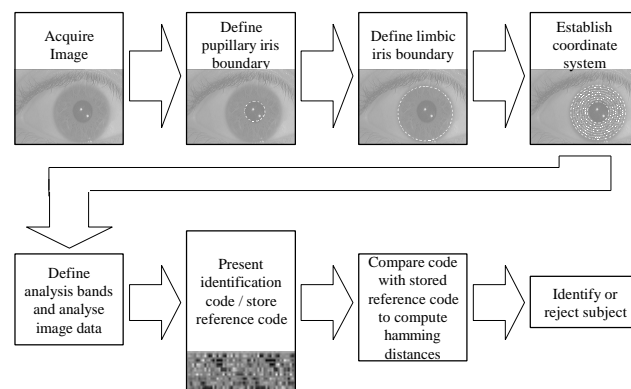

Figure 1   Block diagram of Dr. Daugman's model

3.1   Acquire Image

In practical application of a workable system, an image of the eye to be analyzed must be acquired first in digital form suitable for analysis as shown in Figure 2
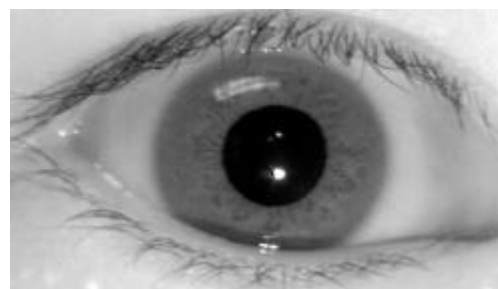

Figure 2   An eye sample containing the image of an iris.

3.2   Image Analysis

Iris analysis begins with reliable means for establishing whether an i ris is visible in the video image, and then precisely locating its inner and outer boundaries (pupil and limbus). Because of the felicitous circular geometry of the iris, these tasks can be accomplished for a raw input image $I(x,y)$ by integrodifferential operators that search over the image domain (x,y) for the maximum in the blurred partial derivative, with respect to increasing radius r, of the normalized contour integral of $I(x,y)$ along a circular arc ds of radius r and center coordinates (x_o,y_o):

$$\max_{(r,x_o,y_o)} \left| G_? \, ?r? \, \frac{?}{?r} \oint_{r,x_o,y_o} \frac{I(x,y)}{2?r} ds \right| \tag{1}$$

where * denotes convolution and is a smoothing function such as a Gaussian of scale $?$. The complete operator behaves in effect as a circular edge detector, blurred at a scale set by $?$, that searches iteratively for a maximum contou r integral derivative with increasing radius at successively finer scales of analysis through the three parameter space of center coordinates and radius (x_o,y_o,r) defining the path of contour integration.

3.2.1   Operators for Locating an Iris

At first the blurri ng factor $?$ is set for a coarse scale of analysis so that only the very pronounced circular transition from iris to (white) sclera is detected. Then after this strong circular boundary is more precisely estimated, a second search begins within the confined central interior of the located iris for the fainter pupillary boundary, using a finer convolution scale $?$ and a smaller search range defining the paths (x_o,y_o,r) of contour integration. In the initial search for the outer bounds of the iris, the angula r arc of contour integration ds is restricted in range to two opposing 90° cones centered on the horizontal meridian, since eyelids generally obscure the upper and lower limbus of the iris. Then in the subsequent interior search for the pupillary boundary , the arc of contour integration ds in operator (1) is restricted to the upper 270° in order to avoid the corneal specular reflection that is usually superimposed in the lower 90° cone of the iris from the illuminator located below the video camera. Taking the absolute value in (1) is not required when the operator is used first to locate the outer

boundary of the iris, since the sclera is always lighter than the iris and so the smoothed partial derivative with increasing radius near the limbus is always po sitive. However, the pupil is not always darker than the iris, as in persons with normal early cataract or significant back-scattered light from the lens and vitreous humour; applying the absolute value in (1) makes the operator a good circular edge-finder regardless of such polarity-reversing conditions. With $?$ automatically tailored to the stage of search for both the pupil and limbus, and by making it correspondingly finer in successive iterations, the operator defined in (1) has proven to be virtually infallible in locating the visible inner and outer annular boundaries of irises.

For rapid discrete implementation of the integrodifferential operator in (1), it is more efficient to interchange the order of convolution and differentiation and to concatenate them, before computing the discrete convolution of the resulting operator with the discrete series of undersampled sums of pixel along circular contours of increasing radius. Using the finite difference approximation to the derivative for a discrete series in n,

$$\frac{?G_s(r)}{?r} ? G_?^{(1)}(n) ? \frac{1}{?r}G_?(n?r) ? \frac{1}{?r}G_?((n?1)?r) \qquad (2)$$

where $?r$ is a small increment in radius, and replacing the convolution and contour integrals with sums, we can derive through these manipulations an efficient discrete operator for finding the inner and outer bound aries of an iris:

$$\max_{(n?r,x_o,y_o)} \left| \frac{1}{?r} ?_k \{G_?((n?k)?r) ? G_?((n?k?1)?r)) ?_m I[(k?r\cos(m??) ? x_o),k?r\sin(m??) ? y_o)]\} \right| \qquad (3)$$

where $??$ is the angular sampling interval along the circular arcs, over which the summed $I(x,y)$ pixel intensities represent the contour integrals expressed in (1).

A nonlinear enhancement of this operator mak es it more robust for detecting the inner boundary of the iris. Because the circular edge that defines the pupillary boundary is often very faint, especially in dark-eyed persons, it is advantageous to divide each term in the convolution summation over k in (3) by a further contour integral around a smaller radius *(k-2) r*. This divisor becomes very small and stable as the parameters *(n?r,x_o,y_o)* of contour integration become well-matched to the true location and size of the pupil, and this helps the resultin g sum of ratio terms to achieve a distinctive maximum that reliably locates the pupillary boundary:

$$\max_{(n?r,x_o,y_o)} \left| ?\atop k \left\{ \frac{(G_? ((n ? k)? r) ? G_? ((n ? k ? 1)? r))? \sum\limits_{m} I[(k? r\cos(m??) ? x_o), k? r\sin(m??) ? y_o)]}{? r ? \sum\limits_{m} I[((k ? 2)? r\cos(m??) ? x_o),(k ? 2)? r\sin(m??) ? y_o)]} \right. \right| \qquad (4)$$

In essence, dividing by the second contour integral exploits the fact that the interior of the pupil is generally both homogeneous and dark. This creates a suddenly very small divisor when the parameters (n ? r,x_o,y_o) are optimal for the true pupil, thus producing a sharp maximum in the overall search operator (4).

Using multigrid search with gradient ascent over the image domain *(x,y)* for the center coordinates and initial radius of each series of contour integrals, and decimating both the incremental radius ? r interval and the angular sampling ? ? interval in successively finer scales of search spanning four octaves, these iris locating operations become very efficient without loss of reliability. The total processing time on a RISC-based CPU for iris detection and localization to single-pixel precision using such operators, starting from a 640 x 480 image, is about one -quarter of a second (250 *m*sec) with optimized integer code.

3.2.2   Assessing Image Quality, Eyelid Occlusion, and Possibility of Artifice

The operators described above for finding an iris also provide a good assessment of "eyeness", and of the auto-focus performance of the video camera. The normally sharp boundary at the limbus between the iris and the (white) sclera generates a large positive circular edge. If a derivative larger than a certain criterion is not detected by the searching operator using the contour integral defined in (3), then it suggests either that no eye is present, or that it is largely obscured by eyelids, or that it is in poor focus or beyond resolution. In practice the automatic identifying system that has been built continues to grab image frames in rapid succession until several frames in sequence confirm that an eye is apparently present, through large values being found by operator (3), and through large ratios of circular contour integrals being found on either side of the putative limbus boundary. Excessive eyelid occlusion is alleviated in cooperating Subjects by providing live video feedback through the lens of the video camera into which the Subject's gaze is directed, by means of a miniature liquid-

crystal TV monitor displaying the magnif ied image through a beam splitter in the optical axis.

A further test for evidence that a living eye is present exploits the fact that pupillary diameter relative to iris diameter in a normal eye is constantly changing, even under steady illumination. Continuous involuntary oscillations in pupil size, termed hippus or pupillary unrest, arise from normal fluctuations in the activities of both the sympathetic and parasympathetic innervations of the iris sphincter muscle. These changes in pupil diameter rel ative to iris diameter over a sequence of frames are detected by the discrete operators (4) and (3) respectively. In order to compute a "hippus measure" defined as the coefficient of variation (standard deviation divided by mean) for the fluctuating time series of these diameter ratios. Together with the accompanying elastic deformations in the iris texture itself arising either from normal hippus or from a light-driven pupillomotor response, these fluctuations could provide a test against artifice (such as a fake iris painted onto a contact lens) if necessary in highly secure implementations of this system.

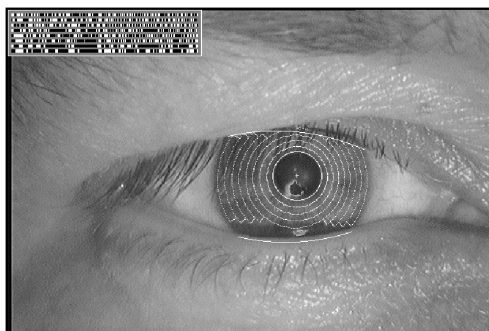### 3.2.3 Doubly Dimensionless Projected Polar Coordinate System

Figure 3 Demarcated zones of analysis and illustration of a computed iris code.

Zones of analysis are established on the iris in a doubly dimensionless projected polar coordinate system. Its purpose is to maintain reference to the same regions of iris tissue regardless both of pupillary constriction and overall iris image size, and hence regardless of distance to the eye and video zoom factor. This pseudo polar coordinate system is not necessarily concentric, since for most eyes the pupil is not central in the iris. (Typically the pupil is both nasal to, and inferior to, the center of the iris, and it is not unusual for its displacement to be as great as 15%.) The stretching of the elastic trabecular meshwork of the iris from constriction of the pupil, is intrinsically modeled by the doubly dimensionless projected coordinate system as the stretching of a homogeneous rubber sheet, which has the topology of an annulus

anchored along its outer perimeter, with tension controlled by an off-centered interior ring of variable radius.

The homogeneous rubber sheet model assigns to each point in the iris, regardless of size and pupillary dilation, a pair of dimensionless real coordinates $(r,\emptyset)$ where r lies on the unit interval $[0,1]$ and ? is the usual angular quantity that is cyclic over $[0,2?]$. The remapping of the iris image $I(x,y)$ from raw coordinates (x,y) to the doubly dimensionless non-concentric polar coordinate system (r,?) can be represented as

$$I(x(r?,), y(r,?)) ? \ I(r,?) \quad (5)$$

where $x(r,?)$ and $y(r,?)$ are defined as linear combinations of both the set of pupillary boundary points $(x_p(\emptyset), y_p(\emptyset))$ around the circle that was found to maximize operator (4), and the set of limbus boundary points along the outer perimeter of the iris $(x_?)(?), y_?(?)$ bordering the sclera, that was found to maximize operator (3):

$$x(r,?) ? (1 ? r)x_P(?) ? rx_?(?) \qquad (6)$$
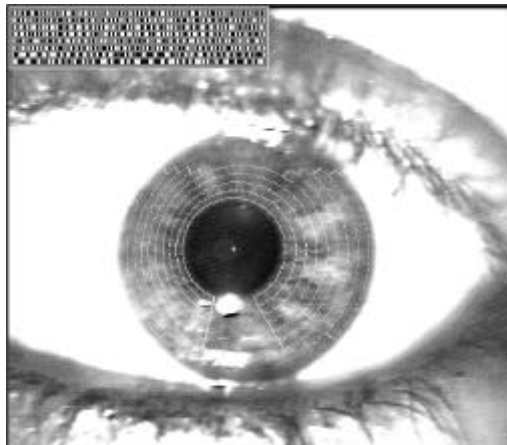
$$y(r,?) ? (1 ? r)y_P(?) ? ry_?(?) \qquad (7)$$

Figure 4   Demarcated zones of analysis and illustration of a computed iris code.

Demarcations of the zones of analysis specified in this projected doubly dimensionless coordinate system, for two sample close-up iris images, are illustrated in Figures 3 and 4. These zones of analysis are assigned in the same format for all eyes and are based on a fixed partitioning of the dimensionless polar coordinate system. But of course for any given eye their affine radial scaling depends on the actual pupillary diameter (and possible offset) relative to the limbus boundary as determined by operators (3) and (4). The zones of analysis always exclude a region at the top of the iris where partial occlusion by the upper eyelid is common and a 45° notch at the bottom where there is a corneal specular reflection from the filtered light source that illuminates the eye from below. (Illumination at an angle is desirable to deflect its specular reflection from eyeglasses,

which persons are not asked to remove. The much greater curvature of the cornea compared with that of spectacle lenses, however, prevents elimination of the illuminator's first Purkinje reflection from the moist lower front surface of the cornea or of contact lenses; this necessitates the exclusion notch in the zones of analysis near the 6-o'clock position.)

Rotation invariance to correct for head tilt and cyclovergence of the eye within its orbit is achieved in a subsequent stage of analysis of the iris code itself. The overall recognition scheme is thus invariant under the Poincaré group of transformations of the iris image: planar translation, rotation (due to cyclovergence and tilt of the head), and dilation (due both to imaging distance and video zoom factor). Through the doubly dimensionless coordinate system, the constructed iris code is also invariant under the non-affine elastic distortion (or projected conic transformation) that arises from variable pupil constriction.

3.2.4   Code Construction and Entropy Measures

3.2.4.1   The 256-Byte Iris Code

The 2-D Gabor filters used for iris recognition as shown in Figure 5 are defined in the doubly dimensionless polar coordinate system (r, $?$) as follows:

$$G(r,?) ? e^{?i? (? ??_o)} e^{?(r? r_o)^2 / ? ^2} e^{?(? ??_o)^2 / ? ^2} \qquad (8)$$

Both the real and imaginary members of such quadrature filters are employed, so the resulting image projections are complex. The real parts of the 2-D Gabor filters are slightly adjusted through truncation to give them zero volume, and hence no DC response, so that computed iris code bits do not depend upon strength of illumination. (The imaginary parts of the filters inherently have no DC response because of odd symmetry.) The parameters $?$ and $?$ co-vary in inverse proportion to $?$ to generate a self-similar, multi-scale

Figure 5   Gabor Filter at 0 degree Orientation

wavelet family of 2-D frequency-selective quadrature filters with constant logarithmic

bandwidth, whose locations, specified by $?_o$ and r_o, range across the zones of analysis of the iris.

Each bit h in an iris code can be regarded as a coordinate of one of the four vertices of a logical unit square in the complex plane (Figure 6). It is computed by evaluating, at one scale of analysis, the sign of both the real and imaginary parts of the quadrature image projections from a local region of the iris image $I(?,?)$ onto a particular complex 2-D Gabor filter:-

$$h_{\mathrm{Re}} \; ? \; 1 \text{ if } \mathrm{Re} \underset{? \; ?}{? ?} e^{? \, iw(?_o??)} e^{? (r_o??)^2 / ?^2} e^{? (?_o??)^2 / ?^2} I(?,?)?d?d? \; ? \; 0 \qquad (9)$$

$$h_{\mathrm{Re}} \; ? \; 0 \text{ if } \mathrm{Re} \underset{? \; ?}{? ?} e^{? \, iw(?_o??)} e^{? (r_o??)^2 / ?^2} e^{? (?_o??)^2 / ?^2} I(?,?)?d?d? \; ? \; 0 \qquad (10)$$

$$h_{\mathrm{Im}} \; ? \; 1 \text{ if } \mathrm{Im} \underset{? \; ?}{? ?} e^{? \, iw(?_o??)} e^{? (r_o??)^2 / ?^2} e^{? (?_o??)^2 / ?^2} I(?,?)?d?d? \; ? \; 0 \qquad (11)$$

$$h_{\mathrm{Im}} \; ? \; 0 \text{ if } \mathrm{Im} \underset{? \; ?}{? ?} e^{? \, iw(?_o??)} e^{? (r_o??)^2 / ?^2} e^{? (?_o??)^2 / ?^2} I(?,?)?d?d? \; ? \; 0 \qquad (12)$$

Thus a single complex 2-D Gabor filter (13), having a particular set of size and position parameters $(r_o, ?_o, ?, ?, ?)$ in the dimensionless iris domain $(r,?)$, performs a coarse phase quantization of the local texture signal by approximating it as one vertex (h_{Re}, h_{Im}) of the logical unit square associated with this filter through conditionals (9) - (12). The time required for computing a complete iris code of 2,048 such paired bits (256 bytes) on a RISC-based CPU, once an iris has been located within the image,

Figure 6   Phase-Quadrant Iris Demodulation Code

is about one-tenth of a second (100 msec) with optimized integer code.
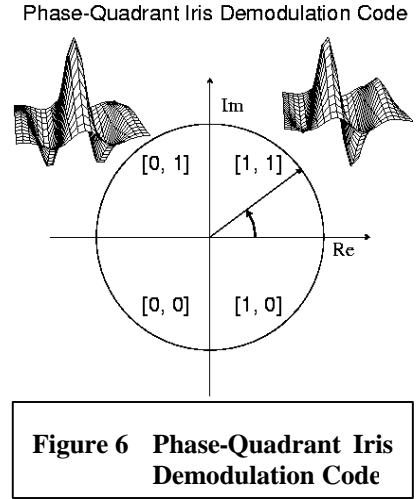
3.2.4.2 Commensurability of Iris Codes

A critical feature of this coding approach is the achievement of commensurability among iris codes, by mapping all irises into a representation having universal format and constant length, regardless of the apparent amount of iris detail. In the absence of commensurability among the codes, one would be faced with the inevitable problem of comparing long codes with short codes, showing partial agreement and partial disagreement in their lists of features. It is not obvious mathematically how one would make objective decisions and compute confidence levels on a rigorous basis in such a situation. This difficulty has hampered efforts to automate reliably the recognition of fingerprints. Commensurability facilitates and objectifies the code comparison process, as well as the computation of confidence levels for each decision. It thereby greatly increases both the speed and the reliability of iris recognition decisions.

3.2.4.3 Bitwise Entropy and Iris Variation

A primary question is whether there is independent variation in iris detail, both within a given iris and across the human population. Any systemat ic correlations in iris detail across the population would undermine the uniqueness of an iris code. Similarly, any systematic correlations within an iris would reduce its statistical complexity, or dimensionality, and thus also undermine its uniqueness.

A code of any length has maximum information capacity if all its possible states are equiprobable. This reflects the fact that the Shannon entropy measure

$$S \ ? \ ? \sum_{j?1}^{n} P_j \log_2 P_j \qquad\qquad\qquad\qquad (13)$$

for the probability of each of the n states and with

$$\sum_{j?1}^{n} P_j \ ? \ 1 \qquad\qquad\qquad\qquad (14)$$

is maximum when for all j,

$$S \ ? \ ? \sum_{j?1}^{n} P_j \log_2 P_j \qquad\qquad\qquad\qquad (15)$$

By construction the 2-D Gabor filters (8) have no DC response in either their real or imaginary parts, as noted earlier. This eliminates possible dependency of the computed code bit conditionals (9) - (12) on mean illumination of the iris and on its contrast gain, and it also renders equiprobable the four vertices of the logical unit square (h_{Re}, h_{Im}) associated with each 2-D Gabor filter. As a consequence of analyzing the iris texture with filters lacking any DC response, the iris code has the property of encoding zero-crossings, which are known to be exceedingly rich in information for band limited signals.

The variation among iris code bits as defined above in (9) - (12) was tracked both across bit location within the code and across a population of 592 different iris codes. For each of 128 code bit locations, drawn from all parts of the iris code, Figure 7 plots the probability of a set bit. The graph shows that this is fairly equiprobable across all code bit locations, and that it remains close to one-half.
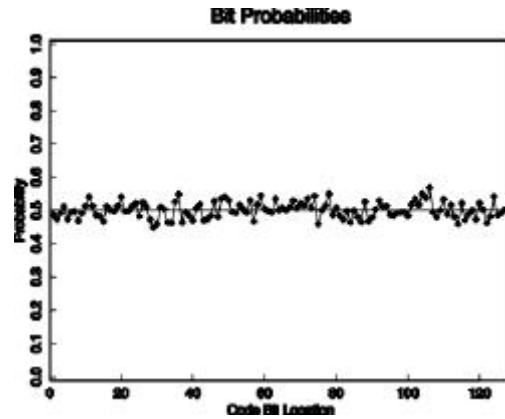
Figure 7 Equiprobable variation of iris code bits, for each of 128 code bit locations, across a population of 592

(Mean of the means is.) The flatness of the graph reflects the existence of independent variation in the detailed iris texture, both across an iris and across the human population studied. Across the population, the constant independent probability of any given code bit being set (i.e. the full equivocation entropy between iris codes) presumably reflects the absence of genetic penetrance in the detailed morphogenesis of this tissue, in favor of stochastic or chaotic processes. Any systematic feature, say at the 12-o'clock position in the iris, would have caused systematic deviation in Figure 3 for the bit probabilities derived from that region. This graph's proximity to a probability of one-half establishes that, since very nearly $?=1-?$, the iris code is bitwise a maximum entropy code.

3.2.4.4   Number of Independent Degrees-of-Freedom in an Iris Code

Although there are 256 bytes or 2,048 bits in any given iris code, such a code possesses far fewer than 2,048 independent binary degrees-of-freedom. One reason is that there are substantial radial correlations within an iris.

For example, a given furrow or ciliary process tends to propagate across a significant radial distance in the iris, e xerting its influence on several remote parts of the code, thus reducing their independence. Similarly, a feature such as a furrow influences different parts of the code associated with several different scales of analysis, since the Fourier spectrum of such a punctuate feature can span several octaves. Finally, inherent correlations are introduced by the band pass property of the 2-D Gabor filters, specifically by the finite bandwidth determined by parameters in (8).

The number of independent degrees-of-freedom typically remaining in an iris code after both of these sources of correlation have been factored in those arising from the 2-D Gabor filters and those inherent within an iris, can be estimated by examining the distribution of Hamming distances computed across a population of unrelated iris codes. Comparing each pair of iris codes A and B bit-by-bit,

Figure 8   Distribution of Hamming distances between unrelated iris codes.

their normalized Hamming distance HD is defined here as the fraction of disagreeing bits between them:

$$HD ? \frac{1}{2048} \sum_{j?1}^{2048} A_j (XOR) B_j \qquad\qquad (15)$$

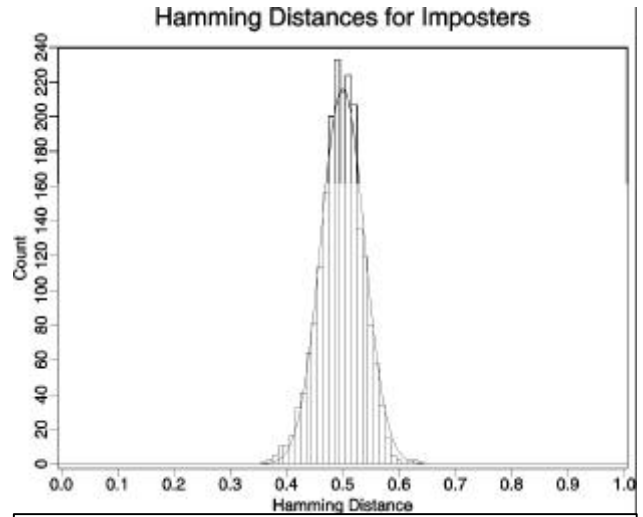where the Boolean operator (XOR) equals 1 if and only if the two bits A_j and B_j are different.

The actual distribution of observed Hamming distances between codes for different irises is shown in Figure 8, which is generated from 2,064 complete comparisons between unrelated pairs of iris codes. This empirical distribution has a standard deviation of $\sigma = 0.038$, with a mean of $\mu = 0.497$. Since the standard deviation of a binomial distribution is given by $\sigma = (pq/N)^{1/2}$ (where $q=1-p$), this distribution of Hamming distances would correspond to a binomial process with N=173 Bernoulli trials per run. Given the estimate of roughly a four-sample correlation distance introduced by the 2-D Gabor encoders, we can now estimate that a bound on the "source entropy", reflecting the number of degrees-of-freedom of variation typical of iris texture resolved to 2,048 samples, would be something like 690 bits.

3.2.4.5 Statistical Decision Theory

The problem of recognizing the signature of a given iris as belonging to a particular individual, either after exhaustive search through a large database or just by comparison with a single authentication template, can be formulated within the framework of statistical decision theory. This framework also resolves the critical problem of assigning a confidence level to any such recognition decision. By this approach we can convert the problem of pattern recognition into a much more expedient task, which is the execution of a simple test of statistical independence.

Chapter 4

4 Implementation of Dr J. Daugman's System

Before implementing the actual iris recognition system, we take a perspective look at the entire process of obtaining iris code from input images. Two most important factors to be concerned are the method of acquiring eye images in digital form and the programming language where the algorithm is going to be written in. With the support of Dr Brian Lovell and the generosity of the department, we were given state of the art machines and all the facilities necessary for the purpose of this th esis.

4.1 Design Decisions

In order to acquire the image of an eye with clear iris pattern, a Sony Video camera was connected to the build-in video capture card in our IBM PC machine. As a reminder to the reader, the thesis objectives, as stated in Chapter 1, were to construct a working iris recognition system. However, focus will be stressed on the software algorithm implementation, that is, we can assume eye images are captured in an appropriate manner without great difficult. Detail of image acquirement would not be stated.

4.2   Acquiring Image

For the purposes of this thesis, the conversion of input images to digitized form is necessary. We were lucky enough to be given state of the art computers with Pentium III – 450Mhz processor and video capture capability that makes image acquiring much more easily.

4.3   Image Analysis

Image analysis requires a lot of complex mathematics calculations, which is why Matlab, with its powerful mathematics, signal and image processing capabilities, made itself the first choice of platform for developing algorithm

4.3.1   Defining Pupillary Iris Boundary

The first procedure in the whole image analysis is to define the pupillary iris boundary. The inner boundary of the iris, forming the pupil, can be accurately determined by exploiting the fact that the boundary of the pupil essentially a circular edge. The pupil is generally dark while the iris is lighter, with varied pigmentation.

When an image is imported into Matlab (Figure 9), the image is firstly transformed into a 256 level grayscale image between 0 being black, and 255 being white (Figure 10). Pupillary boundary is detected as an abrupt and sudden change

Figure 9   Original image

in brightness when summed along a circle whose radius steadily increasing. This sudden change will be maximum when the circle has its center near the true center of the pupil, and when its radius matches the true radius of the pupil. Thus, the image processing problem of finding the pupil can be formulated as an optimization problem, in which a series

Figure 10   Greyscale image

of "exploding circles" (steadily increasing radii) are positioned with the center coordinates located at each one of the number of trail points on a grid.
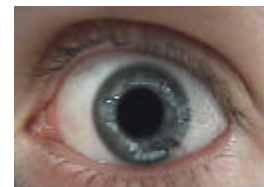
However, if every points in an image $I(x,y)$ are used as a test center coordinate, the process time would be very long. Another way of shortening the time of this process is to make a good approximation of the center first, then start moving out from this estimated center.

In order to obtain this estimated center by weight centroid, the image is filtered (Figure 11) using histogram equalization method then thresholding, by setting intensity which is greater than intensity threshold *a* to 255, white, and intensity less than *b* to black, 0. Then a circle mask of arbitrary area of $r^2 * ?$ is applied only the dark mass centroid in the pupil are left. Then an estimated center is found on the final filtered image.

Figure 11   Histogram Equalized ？ Thresholded images ？ Circle masked image

After the estimated center of pupil was found, all points on a square of arbitrary size *n* centered at this point were used as test centers. For each exploding circle, and for each value for its radius, the total image brightness is summed over fixed number of points lying on this circle (Using a constant number of points on each circle, typically 128, avoids an automatic increase in the summed brightness

Figure 12   Pupillary Iris Boundary

simply due to increasing circumference.). The system searches for the maximum rate of change in this quantity as the radius expand. For the candidate circle that best describes the papillary boundary, there will be a sudden "spike" in the rate -of-change of luminance summed around its perimeter, when its radius just matches that of the papillary boundary. This "spike" will be larger for a circle that shares the pupil's center coordinates and radius, then for all other circles. In this manner, the problem of locating the pupil (Figure 12) has been converted into an optimization problem in
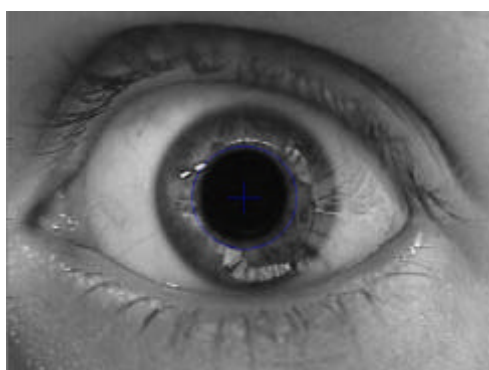
which a three-perimeter space is searched for the best combination of circle center coordinate (x_o, y_o) and radius r.

4.3.2 Defining Limbic Boundary

The limbic boundary is found under same manner as finding the pupillary iris boundary. The gradients of sum of all increasing arc intensities centred on the 25 test centres are plotted as shown

Figure 13   Gradients of sum of intensities around arc for 25 test centres vs. Radius

in Figure 14. However, the fact that the iris is less uniform than the pupil, and have large "circular edges", instead of specifying a series of "exploding circles", "exploding pie wedges" in the horizontal meridian are used; hence avoiding upper and lower eyelids occlusion.
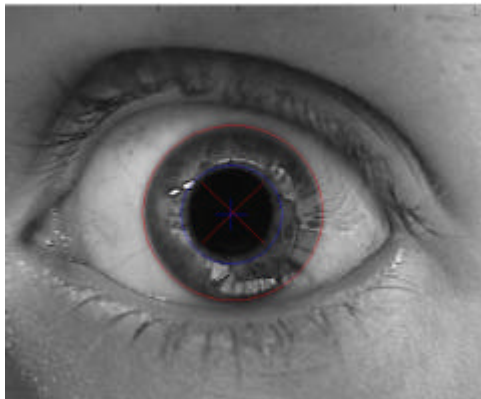

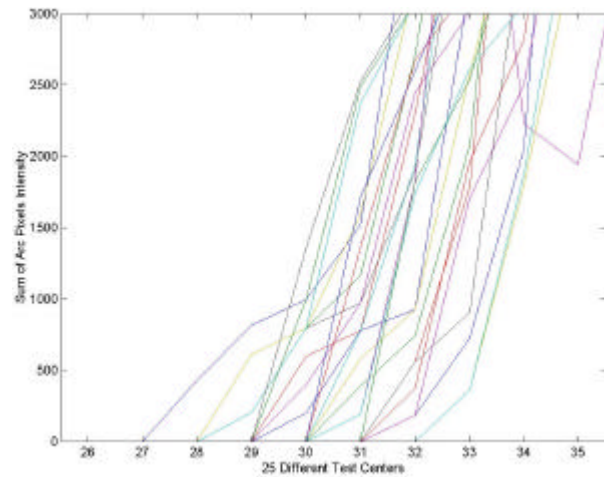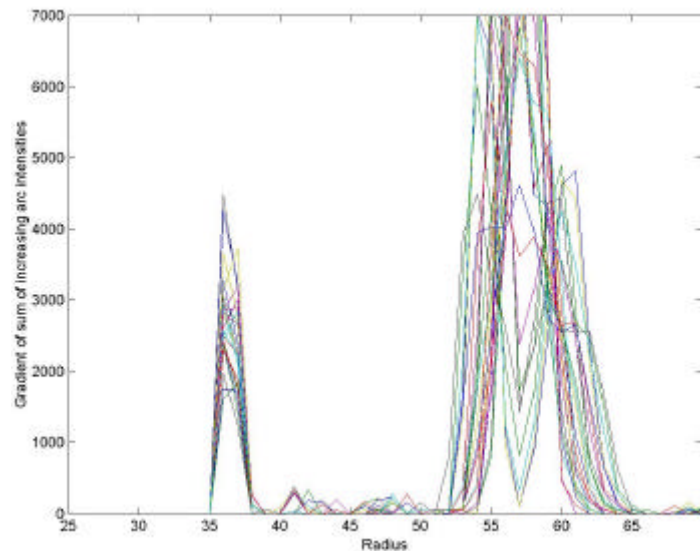**Figure 15   Both   Pupillary   Iris   Boundary   &   Limbic**

Figure 14   Gradients of sum of intensities around arc for 25 test centres vs. Radius

4.3.3   Establishing Coordinate System

Perhaps the main feature of Daugman's approach to iris identification is that the iris codes it generates are commensurable, which simplifies the process of comparing them. This is possible partly because all human irises are roughly toroidal in shape. As such, the iris is well suited for mapping into a normalized polar coordinate system. In this new system, all points within the boundaries of the original iris image are located by the coordinates ? , ranging from 0 to 1 (0 being the inner boundary and 1 the outer boundary), and ? , ranging from 0 to 2?. As the inner boundary of the iris is not usually concentric with the outer boundary, it is necessary to use a linear stretch transformation to ensure that the location of a point in the new coordinate system corresponds to the distance between its location in the old system and the boundaries of the iris. The result of this transformation is that all iris images are mapped into the same area in the polar coordinate space, although the original images may be of different sizes, resolutions, and may be more or less concentric to begin with.

4.3.4   256 bytes Code Construction

Due to the difficulties aroused during construction of polar coordinate system, there was no iris code constructed up to the due date of thesis written report. However, the following is another example of automatic boundary detection (Figure 17) with its image reconstructed on a polar coordinate systems (before being gabor filtered).
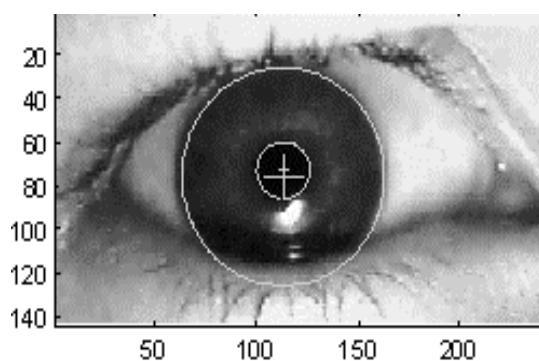

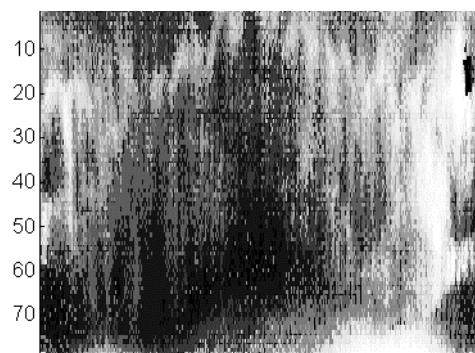**Figure 16 An example of eye image with both boundaries detected**

Figure 17   The example on the left hand side as seen in stretched polar coordinates.

Chapter 5

5 Design Review

Unfortunately, up to the date of submission of the thesis report, a complete Iris Recognition system was not fully implemented. Only inner and outer iris boundaries detection algorithm were completed due to various reasons. One of the major reasons behind this was the fact that iris recognition is still an uncommon, new and expensive technology, which was patented by Dr J. Daugman.

I personally tried to contact *Iriscan Inc. Corporate* and *Neurotechnologija, Ltd*, who both have commercial iris recognition system, however they have never replied my enquiries and email. This made it extremely hard to obtain insight technical information in how it should be approached

5.1   Results

With the success of developing a working boundaries detecting algorithm, a total of twenty images were tested.

Figure 18   Results of 5 eyes iris boundaries detection.
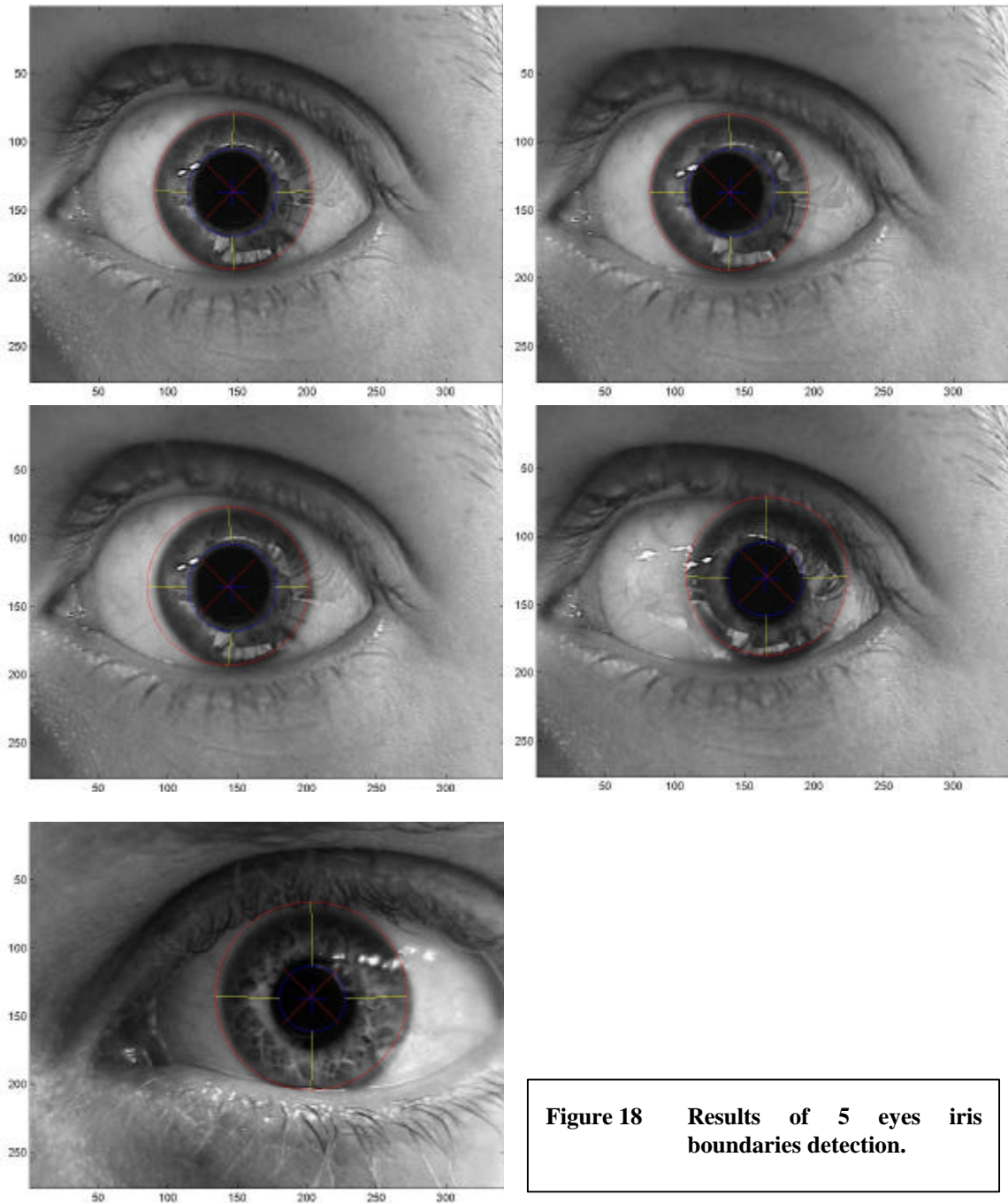
From the results above, further analysis can be made to complete an iris recognition algorithm.   Polar coordinates stretching, gabor-filtered of code extraction, construction and confidence level accept/reject decision making are still needed to be

studied. Moreover, it is important to note that with better quality of input images, algorithm can be highly reduced and improve in speed and reliability.

Chapter 6

6   Conclusions

6.1   Summary and Conclusions

This thesis has presented an overview of Iris Recognition technology which is not only related to the filed of personal identification, and more specifically to the field of automated and efficient identification of humans by biometric indicia.

A software algorithm capable of providing some of Dr. J. Daugman's theory behind Iris Recognition has been specified, designed and implemented. Although some aspects of the project implementations were incomplete, this project may be considered partially successful,.

Areas in which the algorithm is needed to be continue developed and improved had been outlined, and the potentials of utilizing Iris Recognition was examined.

Appendix A

Schematics

Due to the nature of the thesis, no schematic diagram is needed.

Appendix B

Source Code

The following is the main program written in Matlab Release 13 Version 5.3

```
function iris(filename);

im=(rgb2gray(imread(filename)));
im=im(13:288, 1:342);
j=double(im);
[d1 d2]=size(j);
f=0;

%stand out iris-pupil by contrasting
LOW=3;
HIGH=175;
for loop=1:2:LOW*2
   for loop1=1:d1
      for loop2=1:d2
         if j(loop1,loop2)<LOW+loop
            j(loop1,loop2)=0;
         elseif j(loop1,loop2)>HIGH-loop
            j(loop1,loop2)=255;
         else
            j(loop1,loop2)=round(j(loop1,loop2)/(HIGH-LOW-
2*loop)*255);
         end
      end
   end
end

% filter bright pixels by using threshold brightness
threshold=200;
%f=f+1; figure(f), imshow(j), imagesc(j);
```

```matlab
pupil= (j < threshold);
%f=f+1; figure(f), imshow(pupil), imagesc(pupil);


%filtering using area of a whole circle
diameter=33;
mid=(diameter+1)/2;
bound=mid-1;
con=7;
dif=(con+1)/2-1;
result=zeros(d1-mid, d2-mid);
circle=imcircle(diameter);
replace=imcircle(con);
area=(diameter/2)^2*pi;
for loop1 = 1 : d1
    for loop2 = 1 : d2
        if (loop1<mid | loop1>d1-mid | loop2<mid | loop2>d2-mid)
            result(loop1,loop2)=0;
        else
            acc=0;
            compare=pupil(loop1-bound : loop1+bound, loop2-bound :
loop2+bound);
            prod = circle.*compare;
            acc=sum(sum(prod));
            if acc / area > 0.85
                result(loop1-dif: loop1+dif, loop2-dif: loop2+dif) =
ones(con,con);
            else
                result(loop1,loop2)=0;
            end
        end
    end
end

iris=result;
[d1 d2]=size(iris);

%approximate center using weight centroid of pixels
column_weights = [1:d2] .* sum(iris);
column_centroid = round(sum(column_weights(:)) / sum(iris(:)));
row_weights = [1:d1] .* sum(iris, 2)';
row_centroid = round(sum(row_weights(:)) / sum(iris(:)));
f=f+1; figure(f), imshow(im),imagesc(im);pixval;
%line([column_centroid, column_centroid], [1, d1]);
%line([1, d2], [row_centroid, row_centroid]);

%darken pupil
im2=im;
for loop=1:5
   im2=histeq(im2);
   for loop1=1:d1
      for loop2=1:d2
         if im2(loop1,loop2)<50+loop*10
            im2(loop1,loop2)=0;
         elseif im2(loop1,loop2)>160-loop*10
            im2(loop1,loop2)=255;
         end
      end
   end
end
```

```matlab
%find boundary of pupil using sudden change in sum of brightness of
concentric circles
im2=double(im2);
pupilbound=73;
centers=0;
dev=2;
pupilser=zeros((dev*2+1)^2, (pupilbound+1)/2);
for loop1=-dev:dev
   for loop2=-dev:dev
      centers=centers+1;
      for loop3=1:2:pupilbound
         circle=double(bwperim(imcircle(loop3)));
         pupilser(centers,(loop3+1)/2) =
sum(sum(im2(row_centroid+loop1-(loop3-1)/2:row_centroid+loop1+(loop3-
1)/2 , column_centroid+loop2-(loop3-
1)/2:column_centroid+loop2+(loop3-
1)/2).*circle))/sum(sum(circle))*128;
      end
   end
end

pupilser=pupilser';
inner=zeros((pupilbound+1)/2, (dev*2+1)^2);
for loop1=1 : (dev*2+1)^2
   check=0;
   radius=-1;
   for loop2=1 : (pupilbound+1)/2
      radius=radius+1;
      check=check+pupilser(loop2,loop1);
      if check > 0
         inner(loop2,loop1)=check;
         inner(loop2+1:(pupilbound+1)/2,loop1)=0;
%        inner(2,loop1)=radius;
         break;
      end
   end
end

[a1,b1]=max(inner); %a1=max of gradient in each test center, b1 is
the correspond radius
[a2,b2]=max(a1); %a2=max of all the gradients so b2 = correspoding
test center
pupilcenter=b2;
pupilradius=b1(b2);    %b2 is the center and b1(b2) is the center's
radius

pupilcenter_x=column_centroid+(-(dev+1)+rem(pupilcenter,dev*2+1));
pupilcenter_y=row_centroid+-((dev+1)-((pupilcenter -
rem(pupilcenter,dev*2+1)) / (dev*2+1)+1));
hold on; o=0:.01:2*pi; plot(pupilradius*cos(o)+pupilcenter_x,
pupilradius*sin(o)+pupilcenter_y);
ph=line([pupilcenter_x, pupilcenter_x], [pupilcenter_y-10,
pupilcenter_y+10]);
pv=line([pupilcenter_x-10, pupilcenter_x+10], [pupilcenter_y,
pupilcenter_y]);
hold off;
f=f+1; figure(f); plot((pupilser));

%find iris boundary
%darken iris
im2=im;
```

```matlab
for loop=1:5
    im2=histeq(im2);
    for loop1=1:d1
        for loop2=1:d2
            if im2(loop1,loop2)<60+loop*10
                im2(loop1,loop2)=0;
            elseif im2(loop1,loop2)>170-loop*10
                im2(loop1,loop2)=255;
            end
        end
    end
end

im2=double(im2);
irisbound=163;
centers=0;
dev=2;
irisser=zeros((dev*2+1)^2, (irisbound+1)/2);
for loop1=-dev:dev
    for loop2=-dev:dev
        counter=(pupilbound+1)/2-1;
        centers=centers+1;
        jump=0;
        for loop3=pupilbound:2:irisbound
            counter=counter+1;
            jump=jump+2;
            circle=double(bwperim(imcircle(loop3)));
            circle(1:(loop3+1)/2-(pupilbound+1)/2, :)=0;
            circle((loop3+1)/2+(pupilbound+1)/2:loop3, :)=0;
            irisser(centers,counter) = sum(sum(im2(pupilcenter_y+loop1-
((loop3+1)/2-1):pupilcenter_y+loop1+((loop3+1)/2-1) ,
pupilcenter_x+loop2-((loop3+1)/2-1) :
pupilcenter_x+loop2+((loop3+1)/2-1)).*circle))/sum(sum(circle))*128;
        end
    end
end

irisser=irisser';
irisgrad=gradient(irisser');
irisgrad=irisgrad';

[g1,g2]=size(irisgrad);
for loop1=g1
    for loop2=g2
        if irisgrad(loop1,loop2)<0
            irisgrad(loop1,loop2)=0;
        end
    end
end

[i1,j1]=max(irisgrad); %i1=max of gradient in each test center, j1 is
the correspond radius
[i2,j2]=max(i1); %i2=max of all the gradients so j2 = correspoding
test center
iriscenter=j2;
irisradius=j1(j2);

iriscenter_x=pupilcenter_x+(-(dev+1)+rem(iriscenter,dev*2+1));
iriscenter_y=pupilcenter_y+-((dev+1)-((iriscenter -
rem(iriscenter,dev*2+1)) / (dev*2+1)+1));
```

```
figure(1); hold on; o=0:.01:2*pi;
plot(irisradius*cos(o)+iriscenter_x,
irisradius*sin(o)+iriscenter_y,'r');
ih=line([iriscenter_x-20, iriscenter_x+20], [iriscenter_y+20,
iriscenter_y-20]);
iv=line([iriscenter_x-20, iriscenter_x+20], [iriscenter_y-20,
iriscenter_y+20]);
set(ih,'color',[1 0 0]); set(iv,'color',[1 0 0]);
l1=line([pupilcenter_x, iriscenter_x], [pupilcenter_y+pupilradius,
iriscenter_y+irisradius]);
l2=line([pupilcenter_x+pupilradius, iriscenter_x+irisradius],
[pupilcenter_y, iriscenter_y]);
l3=line([pupilcenter_x, iriscenter_x], [pupilcenter_y-pupilradius,
iriscenter_y-irisradius]);
l4=line([pupilcenter_x-pupilradius, iriscenter_x-irisradius],
[pupilcenter_y, iriscenter_y]);
set(l1,'color',[1 1 0]); set(l2,'color',[1 1 0]);set(l3,'color',[1 1
0]); set(l4, 'color',[1 1 0]);
line;
hold off;
```

References

[1]   C. Seal, M. Gifford and D. McCartney, Iris recognition for user validation. British Telecommunications Engineering Journal 16(7), pp. 113 -117, 1997

[2] F. H. Adler, Physiology of the Eye: Clinical Application, fourth ed. London: The C.V. Mosby Company, 1965

[3]   C. Bovik, M. Clark and W. S. Geisler, "Multichannel texture analysis using localized spatial filters," IEEE Trans. Pattern Anal. Machine Intell., vol. 12, pp. 55-73, 1990

[4]   R. Bright, Smartcards: Principles, Practice, Applications. New York: Ellis Horwood, Ltd., 1988

[5]   T. Caelli, "On discriminating visual textures and images," Perception & Psychophysics, vol. 31, pp. 149-159, 1982

[6]   ____, "Energy processing and coding factors in texture discrimination and image processing," Perception & Psychophysics, vol. 34, pp. 349-355, 1983

[7]   M. Clark and A. C. Bovik, "Experiments in segmenting text on patterns using localized spatial filters," Pattern Recognit., vol. 22, pp. 707-717, 1989

[8]   J. M. Coggins and A. K. Jain, " A spatial filtering approach to texture analysis," Pattern Reognit. Lett., vol. 3, pp 195-203, 1985

[9]   J. G. Daugman, "Two-dimensional spectral analysis of cortical receptive field profiles," Vision Res. vol. 20, pp. 847-856

[10]   ____, "Uncertainty relation for resolution in space, spatial frequency and orientation optimized by two-dimensional visual cortical filters," J. Opt. Soc. amer. A, vol. 2, pp. 1160-1169, 1985

[11]   ____, "Complete discrete 2-D Gabor transforms by neural networks for image analysis and compression," IEEE Trans. Acoust., Speech, Signal Processing, vol. 36, pp. 1169-179, 1988

[12]   H. Davson, Davson's Physiology of the eye, 5th ed. London: Macmillan, 1990

[13]   L. Flom and A. Safir, U. S. Patent No. 4641349, U. S. Government Printing Office, Washington, DC, 1987

[14]   F. Galton, "Personal identification and description," Nature, pp. 173-177, June 21, 1988

[15]   J. Ghosh, N. Gopal and A. C. Bovik, "Textured image segmentation using localized receptive fields," i Proc. Int. Joint Conf. Neural Networks, vol. 2, pp. 283-286, 1990

[16]   R. M. Haralick, "Statistical and structural approach to textur e," Proc. IEEE, vol. 67, pp. 786-804, 1979

[17]   R. M. Haralick, K. Shanmugan and I. Dinstein, "Textural features for image classification," IEEE Trans. Syst., Man, Cybern., vol. 3, pp. 610-621, 1973

[18]   L. D. Harmon, M. K. Khan, R. Lasch and P. F. Ramig, "Machine identification of human faces," Pattern Recognit., vol. 13, pp. 97-110, 1981

[19]   K. ain and F. Farrokhnia, "Unsupervised texture segmentation using Gabor filters," Pattern Recognit., vol. 24, pp. 1167-1186, 1991

[20]   F. Logan, "Information in the zero-crossing of bandpass signals," Bell Syst. Tech. J., vol. 56, pp. 487-510, 1977

[21]   S. G. Mallat, "A theory for multiresolution signal decomposition: The wavelet representation," IEEE Trans. Pattern Anal. Machine Intell., vol. 11, pp. 674-693, 1989

[22]   W. W. Peterson, T. G. Birdsall and W. C. Fox, "The theory of signal detectability," Trans. IRE PGIT-4, pp. 171-212, 1954

[23]   M. Porat and Y. Y. Zeevi, "Localized texture processing in vision: Analysis and synthesis in the Gaborian space," IEEE Trans. Biomed. Eng., vol. 36, pp. 115-129, 1989

[24]   J. Rohen, "Morphology and pathology of the trabecular meshwork," in The Structure of the Eye, Smelser, Ed. New York: Academic Press, pp. 335-341, 1961

[25]   Samal and P. A. Iyengar, "Automatic recognition and analysis of human faces and facial expressions: A servey," Pattern Recognit., vol. 25, pp. 65-77, 1992

[26]   Shannon and W. Weaver, Mathematical Theory of Communication, Urbana, IL: Univ. of Illinois Press, 1949

[27]   W. P. Tanner and J. A. Swets, "A decision-making theory of visual detection," Psychol. Rev. vol. 61, pp. 401-409, 1954

[28]   Teuner and B. J. Hosticka, "Adaptive Gabor transformation for image processing," IEEE Trans. Signal Processing, in press, 1993

[29]   M. R. Turner, "Texture descrimination by Gabor functions," Bio. Cybern., vol. 55, pp. 71-82, 1986

[30]   L. Van Gool, P. Dewaele, and A. Oosterlinck, "Texture analysis anno 1983," Comput. Vision, Graphics and Image Processing, vol. 29, pp. 336-357, 1985

[31]   J. G. Daugman, "High confidence Visual Recognition of Persons by a test of statistical independence," IEEE Trans. Pattern Anal. Machine Intell., vol. 15, pp. 1148-1161, 1993

[32]   J. D. Daugman, U. S. Patent No. 5291560, U. S. Government Printing Office, Washington, DC, 1994

[33]   J. D. Daugman, "Complete discrete 2-D Gabor transforms by neural networks for image analysis and compression," IEEE Trans. Acoust., Speech, Signal Processing, vol. 36, pp. 1169-1179, 1988

[34]   http://global.bus.iastate.edu/chu/course/iris.htm

[35]   http://www.cl.cam.ac.uk/users/jgd1000/

[36]   http://www.csee.uq.edu.au/people/staff.html#acad

[37]   http://www.iriscan.com/basis.htm

[38]   http://www.labs.bt.com/library/papers/PAMIpaper/PAMIpaper.html

[39]   http://www.neurotechnologija.com/index.html

[40]   http://www.mathworks.com

[41]   http://www.andrew.cmu.edu/user/jchuang/551/final/finalreport.html

[42]   http://www.cim.mcgill.ca/~mcmordie/